Hindawi
Advances in Civil Engineering
Volume 2019, Article ID 4620430, 15 pages
https://doi.org/10.1155/2019/4620430

Research Article

A New Buckling-Restrained Brace with a Variable Cross-Section Core

Liang Li, Tianhua Zhou, Junwu Chen, and Jianfeng Chen

College of Civil Engineering, Chang'an University, Xi'an 710055, China

Correspondence should be addressed to Liang Li; bright_li@chd.edu.cn

Received 12 August 2019; Revised 12 November 2019; Accepted 21 November 2019; Published 26 December 2019

Academic Editor: Giuseppe Quaranta

In this paper, a new type of buckling-restrained brace characterized by a variable cross-section core (BRB-VCC) is proposed and investigated. The practical design equations of the BRB-VCC are derived based on mechanical and mathematical theories. Six specimens are designed and tested to clarify the mechanical behaviours of the BRB-VCC and to validate the reliability of the proposed equations. The test results show that (1) none of the specimens buckle under compression, as expected, and their ductilities and energy dissipation capacities are satisfactory; (2) the derived formulas are reliable and can be conveniently used in engineering practice; and (3) the yielding displacement of the BRB-VCC is approximately 70% that of the traditional TJ-1 buckling-restrained brace (BRB-TJ-1), which may yield earlier than the BRB-TJ-1 in concrete structures under the action of an earthquake.

1. Introduction

A buckling-restrained brace (BRB) is typically composed of an exterior restrainer and an inner core, and the core does not buckle under compression due to the lateral support of the exterior restrainer [1–3]. The BRB has won the widespread favour of researchers in the past several decades, and many different types of BRBs have been developed by scholars worldwide [4, 5].

In practical engineering, BRBs are widely used in concrete structures, and the failure mode of a concrete structure equipped with BRBs has attracted the attention of many researchers [6–10]. Wu et al. [11] investigated the seismic behaviour of a concrete frame with BRBs by performing a pseudo-static test; the results indicate that the RC frame is damaged earlier than BRBs. Bazaez and Dusicka [12] carried out large-scale experiments on RC frames equipped with diagonal BRBs, and it is found that the concrete components are severely damaged, although the BRBs resist a considerable amount of internal force. Liang and Li [13] presented a comprehensive investigation regarding the design approach and seismic behaviour of a steel-concrete hybrid structure, and the study results suggest that the BRBs effectively increase the stiffness and bearing capacity of the steel frame and decrease the seismic response of the structure in the form of energy dissipation devices.

The destruction of the main concrete structure critically threatens the overall safety of a structure. Therefore, many scholars propose that the damage should be concentrated on the BRBs, and the main structure should remain in the elastic state [14–17]. Tabatabaei et al. [18] developed a new reduced length BRB (RLBRB) by dividing the core into a yielding core and nonyielding nonbuckling core; the results show that the relative length of the yielding core is related to the magnitude of the yielding displacement. Bruneau et al. [19] proposed a damage-controlled design approach, which assumes that all the damages are concentrated on the BRBs and the main vertical loading structure is in the elastic state. Guerrero et al. [20] proposed a performance-based design method of the building reinforced by BRBs, which can be used to promptly calculate the response of low-rise regular buildings. Barbagallo et al. [21] proposed a seismic design method for the concrete reinforcement structure with BRBs based on the EC8 code.

From what has been discussed above, the yielding displacement of a BRB exerts an important influence on the seismic performance of the whole structure. However, the primary concerns of scholars are whether BRBs exhibit stable hysteric behaviour and high ductility [12, 22, 23], and methods to reduce the yielding displacement of BRBs are rarely considered [24–27].

To summarize, the analysis of BRBs with a small yield displacement has important research significance and practical application value. Therefore, a novel buckling-restrained brace with a variable cross-section core (BRB-VCC) is proposed in this paper, whose yielding displacement is reduced because certain parts of the core yield earlier than the remaining parts of the core. The theoretical equations for predicting the yield strength, yield displacement, and axial stiffness of BRB-VCC are derived. Six specimens are tested to clarify the mechanical behaviours and energy dissipation capacities. The reliability of theoretical formulas is verified by experimental results. Finally, the behaviour of BRB-VCC and BRB-TJ-1 is compared by FEM analysis.

2. Composition of a Typical BRB-VCC

As shown in Figure 1, a typical BRB-VCC is composed of an inner core and an outside restraining tube. The core is composed of several segments: connection segment, transition segment, flat-plate segment, and stiffened-plate segment. The axial sliding between the ribs and the tube can occur freely under reciprocating axial force. The ribs are welded on the core plate. It is known that welding process will generate welding stress, which may reduce the fatigue strength of steel. In order to guarantee the quality of the welding seams, the following three methods are suggested in this paper: (1) the welding seams distributed on both sides of the core plate should be welded symmetrically so that the welding deformations may offset each other; (2) block welding sequence should be taken to minimize the welding deformation of the core; and (3) preheating before welding or tempering after welding can also be used to relieve the welding stress.

3. Theoretical Formulas

3.1. Mechanical Model. For simplicity, the bending stiffness of the external tube is assumed to be infinite, and thus, the external tube is replaced by a group of sliding supports in the mechanical model, as shown in Figure 2. The origin of the reference coordinate system, *x-y*, is at the left side of the inner core. The distance x represents the distance from the cross section to the origin. The axial force F is positive during compression and negative during tension.

3.2. Buckling Capacity of the Flat-Plate Segment. As shown in Figure 1, the flat-plate segment is adjacent to the stiffened-plate segment. Thus, the flat-plate can be simplified as a rectangular plate with free unloading edges and fixed loading edges, and the buckling of the flat-plate segment, as shown in Figure 3, should be prevented in the design process.

According to the theory of elastic stability [2], the differential equation of a buckled plate under uniform compression can be expressed as

$$D\left(\frac{\partial^4\omega}{\partial x^4}+2\frac{\partial^4\omega}{\partial x^2\partial y^2}+\frac{\partial^4\omega}{\partial y^4}\right)+q_x\frac{\partial^2\omega}{\partial x^2}=0, \tag{1}$$

where $D = Et^3/12(1-\nu^2)$, which is the flexural rigidity of the plate; E is the elastic modulus; t is the thickness of the flat-plate segment; ν is Poisson's ratio; ω is the deflection function; and q_x is the magnitude of the compressive force per unit length of the edge.

The deflection function ω can be represented by the following expression:

$$\omega = A\left(1-\cos\frac{2\pi x}{l_4}\right), \tag{2}$$

where A is constant and l_4 is the length of the flat-plate segment along the x-axis.

Considering the fixed boundary conditions of the flat-plate segment at the edges, specifically $x=0$ and $x=l_4$, the buckling capacity of the flat-plate segment can be obtained as

$$P_{\mathrm{cr},4} = \frac{\pi^2 bD}{(0.5l_4)^2}, \tag{3}$$

where b represents the width of the flat-plate.

3.3. Axial Strength of the Flat-Plate Segment. The yield strength $F_{\mathrm{y},4}$ and ultimate strength $F_{\mathrm{u},4}$ of the flat-plate segment can be obtained by the following equations [15]:

$$\begin{aligned} F_{\mathrm{y},4} &= f_{\mathrm{y}}A_4,\\ F_{\mathrm{u},4} &= f_{\mathrm{u}}A_4, \end{aligned} \tag{4}$$

where f_{y} is the yield strength of steel, f_{u} is the ultimate strength of the core material, and A_4 is the cross-section area of the flat-plate segment.

3.4. Maximum Length of the Flat-Plate Segment. From equation (3), we find that the buckling capacity of a flat-plate segment is a reciprocal function of the effective length $0.5l_4$. The buckling capacity gradually increases with decrease in the effective length. For a sufficiently short plate, the resistance capacity is determined by the yielding strength of the core. When $F_{\mathrm{y},4} = P_{\mathrm{cr},4}$, the maximum length of the flat-plate segment can be obtained using the following expression:

$$l_{4,\max} = 2\pi\sqrt{\frac{bD}{f_{\mathrm{y}}A_4}}. \tag{5}$$

3.5. Maximum Cross-Section Area of the Stiffened-Plate Segment. The cross-sectional areas of the stiffened-plate segments within the length of l_3 and l_5 are equal (see Figure 1(b)):

$$A_3 = A_5, \tag{6}$$

where A_3 and A_5 denote the cross-section areas of the inner core at segments l_3 and l_5, respectively.

To ensure that the stiffened-plate segment yields before the split of the flat-plate segment, the axial yield strength of

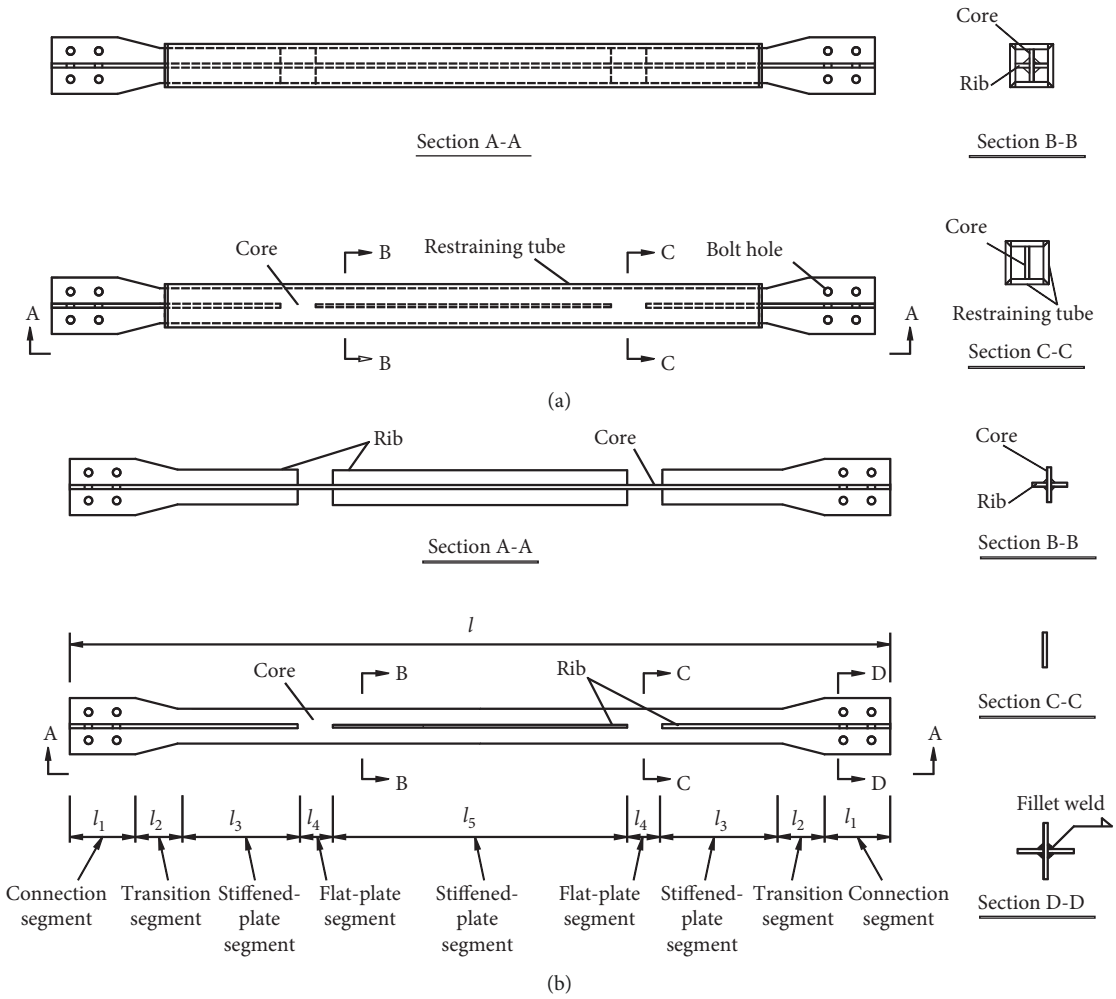

Figure 1: Schematics of a typical BRB-VCC. (a) BRB-VCC. (b) Core.

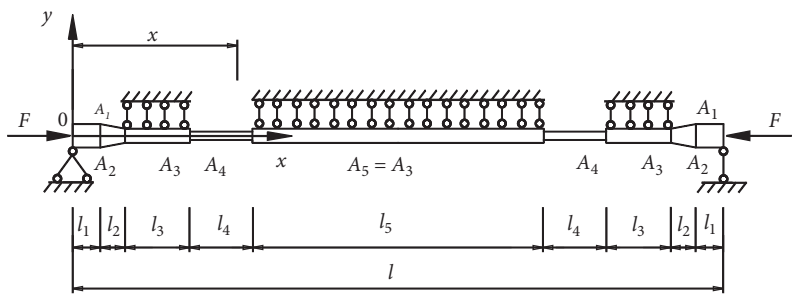

Figure 2: Mechanical model of the core.

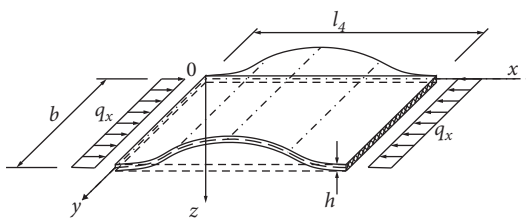

Figure 3: Buckling of the flat-plate segment.

the stiffened-plate segment must be smaller than the ultimate strength of the flat-plate segment:

$$F_{y,3} = F_{y,5} = f_y A_3 = f_y A_5 < F_{u,4}. \quad (7)$$

Therefore, the maximum cross-sectional area of the stiffened-plate segment can be determined:

$$A_{3,\max} = A_{5,\max} = \frac{f_u}{f_y} A_4. \quad (8)$$

3.6. Axial Stiffness of BRB-VCC

3.6.1. Idealized F-δ Diagram. The idealized F-δ diagram of the core is shown in Figure 4. The core initially exhibits a linear relationship between F and δ in the elastic state, in which the elastic stiffness is denoted by k_e. When loading is continued, a point ($F_{y1,}$ δ_{y1}) is reached at which the flat-plate segments yield; this point is called the first yield point. When the load F exceeds F_{y1}, the flat-plate segments reach the strain hardening stage, and the first plastic stiffness is symbolized by k_{p1}. The axial force F is increased until the stiffened-plate segments yield, and this instant represents the second yield point ($F_{y2,}$ δ_{y2}). If loading is continued, the stiffened-plate segments reach the strain hardening stage, and the second plastic stiffness k_{p2} can be identified.

3.6.2. Elastic Stiffness k_e. As shown in Figure 2, the cross-sectional areas $A_{2,x}$ vary along the x-axis, and they can be obtained by

$$A_{2,x} = A_1 - (A_1 - A_3)\frac{x - l_1}{l_2}, \tag{9}$$

where A_1 is the sectional area of the connection segment, l_1 is the length of the connection segment, and l_2 is the length of the transition segment.

By integrating over the length of l_i individually, the axial stretching or shortening of each segment under the action of axial F can be obtained using the following expressions:

$$\delta_i = \int_{\sum l_{i-1}}^{\sum l_i} \varepsilon_i \mathrm{d}x = \frac{Fl_i}{A_i E}, \quad i = 1, 3, 4, 5,$$

$$\delta_2 = \int_{l_1}^{l_1+l_2} \varepsilon_{2,x}\mathrm{d}x = \frac{F}{E}\int_{l_1}^{l_1+l_2}\frac{1}{A_2}\mathrm{d}x = \frac{Fl_2}{E}\frac{\ln A_3 - \ln A_1}{A_3 - A_1}. \tag{10}$$

For each segment, the elastic stiffness can be obtained by the formula

$$k_i = \frac{F}{\delta_i} = \frac{A_i E}{l_i}, \quad i = 1, 3, 4, 5,$$

$$k_2 = \frac{F}{\delta_2} = \frac{E}{l_2}\frac{A_3 - A_1}{\ln A_3 - \ln A_1}. \tag{11}$$

Therefore, the elastic stiffness can be expressed as

$$k_e = \frac{k_1 k_2 k_3 k_4 k_5}{k_1 k_2 k_3 k_4 + 2k_5\left(k_2 k_3 k_4 + k_1 k_3 k_4 + k_1 k_2 k_4 + k_1 k_2 k_3\right)}. \tag{12}$$

3.6.3. First Plastic Stiffness k_{p1}. By integrating over the length of l_4, the change in the plastic length of the flat-plate segment along the axial direction can be obtained:

$$\delta_4^{\mathrm{p}} = \int_{l_1+l_2+l_3}^{l_1+l_2+l_3+l_4} \varepsilon_4 \mathrm{d}x = \int_{l_1+l_2+l_3}^{l_1+l_2+l_3+l_4} \frac{F}{E_t A_4}\mathrm{d}x = \frac{Fl_4}{E_t A_4}, \tag{13}$$

where E_t is the tangent modulus of the core material.

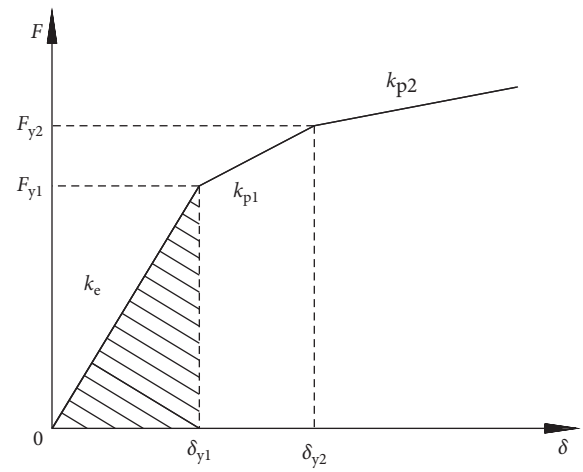

Figure 4: Idealized F-δ diagram of the core.

The plastic stiffness of the flat-plate segment can be expressed as

$$k_4^{\mathrm{p}} = \frac{E_t A_4}{l_4}. \tag{14}$$

Substituting equation (14) in equation (12), the first plastic stiffness of the core equals

$$k_{\mathrm{p1}} = \frac{k_1 k_2 k_3 k_4^{\mathrm{p}} k_5}{k_1 k_2 k_3 k_4^{\mathrm{p}} + 2k_5\left(k_2 k_3 k_4^{\mathrm{p}} + k_1 k_3 k_4^{\mathrm{p}} + k_1 k_2 k_{44}^{\mathrm{p}} + k_1 k_2 k_3\right)}. \tag{15}$$

3.6.4. Second Plastic Stiffness k_{p2}. When the axial force F becomes equal to the second yield force F_{y2}, both the flat-plate segment and the stiffened-plate segment pass into the plastic state. The change in length of the stiffened-plate segment equals

$$\delta_i^{\mathrm{p}} = \frac{Fl_i}{E_t A_i}, \quad i = 3, 5. \tag{16}$$

The plastic stiffness of the stiffened-plate segment is

$$k_i^{\mathrm{p}} = \frac{E_t A_i}{l_i}, \quad i = 3, 5. \tag{17}$$

Therefore, the second plastic stiffness of the core can be obtained using

$$k_{\mathrm{p2}} = \frac{k_1 k_2 k_3^{\mathrm{p}} k_4^{\mathrm{p}} k_5^{\mathrm{p}}}{k_1 k_2 k_3^{\mathrm{p}} k_4^{\mathrm{p}} + 2k_5^{\mathrm{p}}\left(k_2 k_3^{\mathrm{p}} k_4^{\mathrm{p}} + k_1 k_3^{\mathrm{p}} k_4^{\mathrm{p}} + k_1 k_2 k_4^{\mathrm{p}} + k_1 k_2 k_3^{\mathrm{p}}\right)}. \tag{18}$$

4. Design Process

To realize a successful design, the practical design procedure of the inner core, which includes the following steps, is described in a flowchart, as shown in Figure 5.

(1) Select the initial geometric parameters of the BRB-VCC.

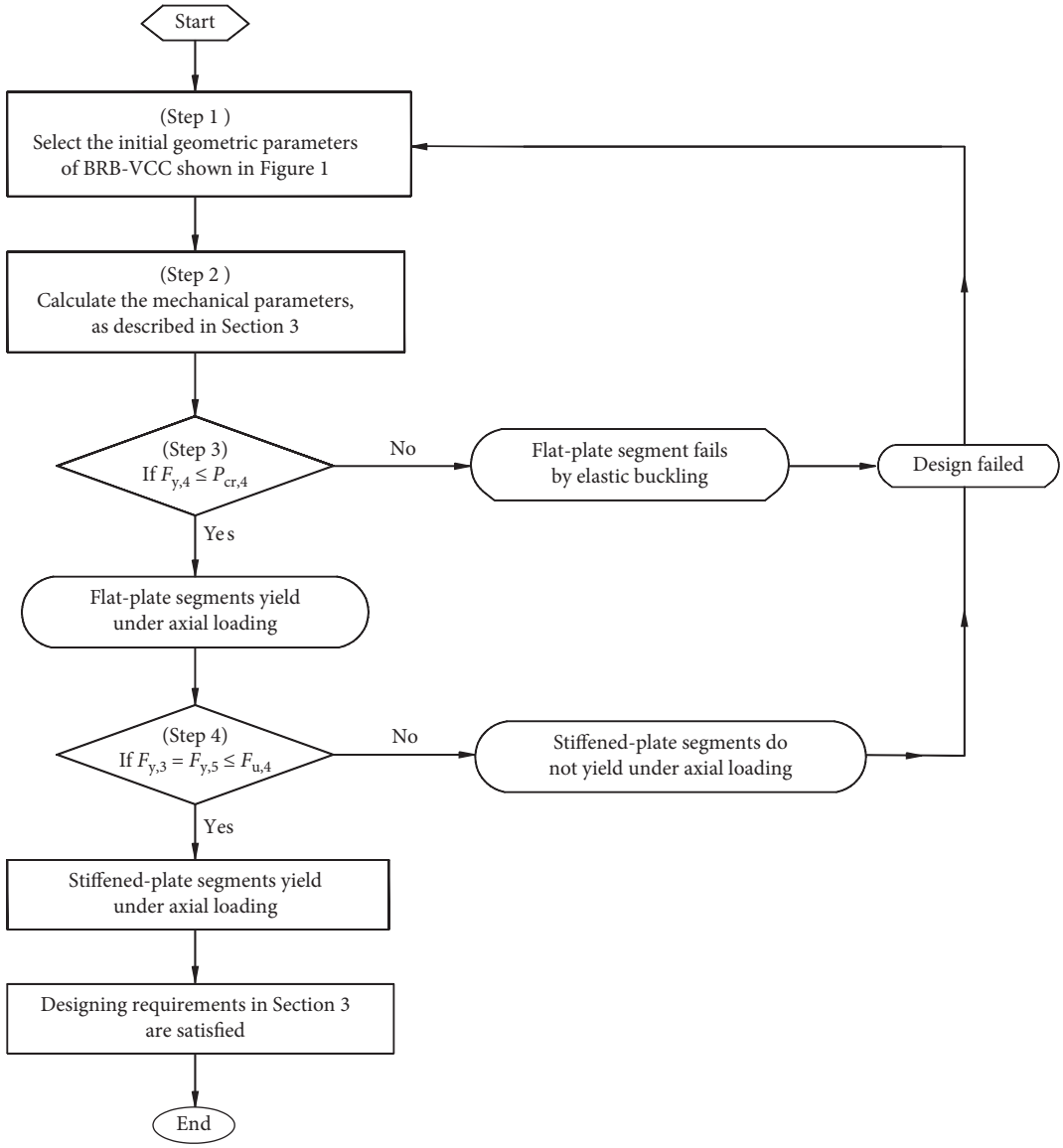

Figure 5: Design process flowchart of BRB-VCC.

(2) Calculate the mechanical parameters by the theoretical formulas presented in Section 3.

(3) Identify the failure mode of the flat-plate segment: if $F_{y4} \le P_{cr,4}$, the BRB-VCC fails by the yielding of the flat-plate segments, as expected. Otherwise, the BRB-VCC fails by the buckling of the flat-plate segments. If so, return to step (1) to reselect the geometric parameters of the flat-plate segment, and iterate until $F_{y4} > P_{cr,4}$.

(4) Check if the stiffened-plate segment yields before the flat-plate segment splits. In this case, if equation (7) is satisfied, the stiffened-plate segments pass into the yield state before the failure of the flat-plate segment. Otherwise, the BRB-VCC fails before the yielding of the stiffened-plate segments. In case this occurs, return to step (1) to reselect the cross section of the flat-plate segment and the stiffened-plate segment, and repeat until $F_{y3} = F_{y4} \le F_{u,4}$ is satisfied.

5. Test Programme

5.1. Specimen Details. The main objective of the specimen design is to make sure that the specimens may reveal the mechanical properties of BRB-VCC, and the dimensions of specimens should guarantee that well ductility and stable hysteretic behaviors can be achieved, and local buckling or overall buckling will not occur. The details of the specimens are shown in Figure 6, and the geometric parameters of the six specimens are listed in Table 1. The properties of the material Q235B used for manufacturing the specimens are listed in Table 2.

5.2. Test Setup and Loading Protocol. As shown in Figure 7, the specimen is loaded at the push-pull fatigue tester (MTS

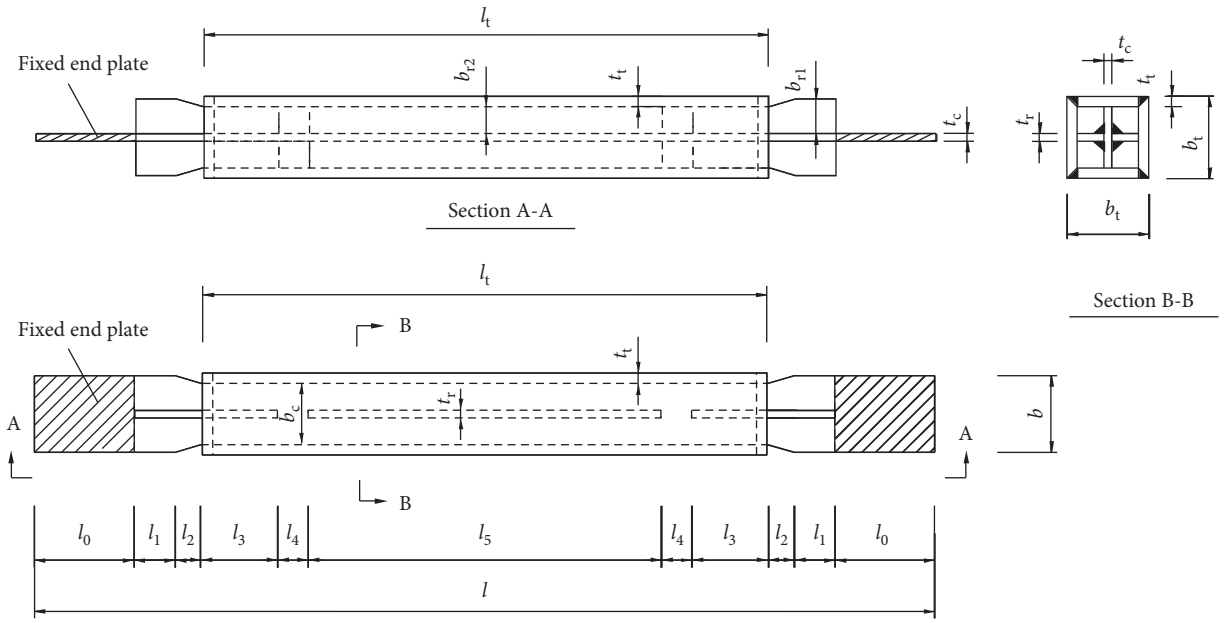

Figure 6: Details of specimens.

Table 1: Geometric parameters of specimens (length unit: mm).

Series	Specimen ID	Length of segments							Rib		Core plate				Restraining tube		
		l	l_0	l_1	l_2	l_3	l_4	l_5	b_{r1}	b_{r2}	t_r	b	b_c	t_c	b_t	t_t	l_t
S-I	BRB-VCC-1 (2, 3)	360	39	16	10	30	10	150	12	9	6	30	24	6	32	4	230
S-II	BRB-VCC-4 (5, 6)	339	20	16	10	30	10	167	10	7	6	26	20	6	28	4	247

Table 2: Material properties of Q235B.

Steel grade	Elastic modulus E (MPa)	Yield strength f_y (MPa)	Yield strain ε_y	Ultimate strength f_u (MPa)	Poisson's ratio ν
Q235B	1.91×10^5	251.3	0.0015	440	0.3

880). The quasi-static loading protocols for the specimens are shown in Figure 8. The axial loading is conducted at a loading speed of 0.1 mm/s. The quasi-static loading protocols for the specimens in the same series are different, as shown in Figure 8. Noticeably, BRB-VCC-1 experiences more loading circles than BRB-VCC-2 and BRB-VCC-3, and BRB-VCC-4 also experiences more loading circles than BRB-VCC-5 and BRB-VCC-6.

5.3. Test Results

5.3.1. Damage Phenomenon. During testing, the inner core can shrink or stretch freely inside the restraining tube. No damage is found on the welding seams between the ribs and the flat-plate. The core does not buckle locally or globally under compression, and the restraining tube does not deform significantly, as shown in Figure 9.

5.3.2. Hysteresis Response. The hysteresis curves of the six specimens are presented in Figures 10 and 11. The energy

Figure 7: Loading of the specimen.

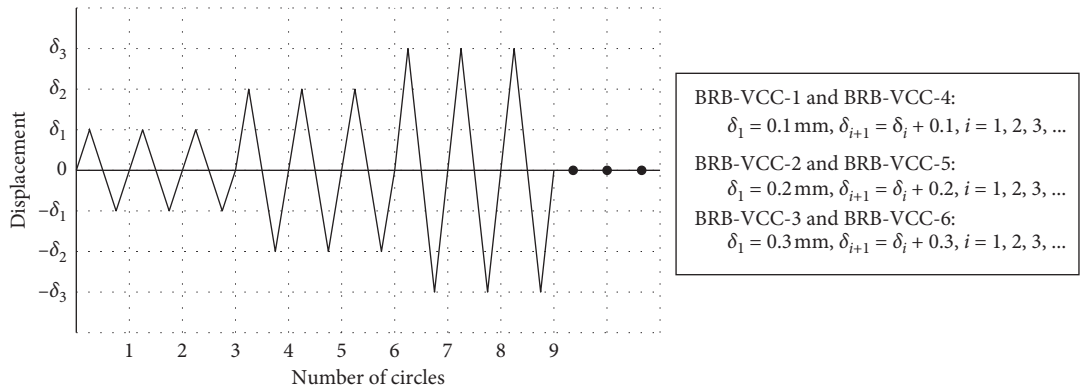

Figure 8: Cyclic loading protocol.

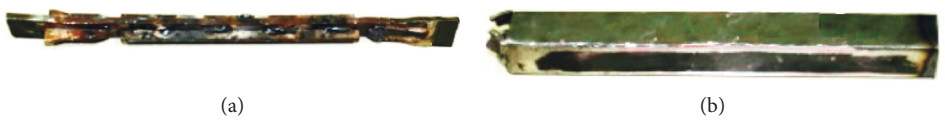

Figure 9: BRB-VCC-1 after test. (a) Core. (b) Restraining tube.

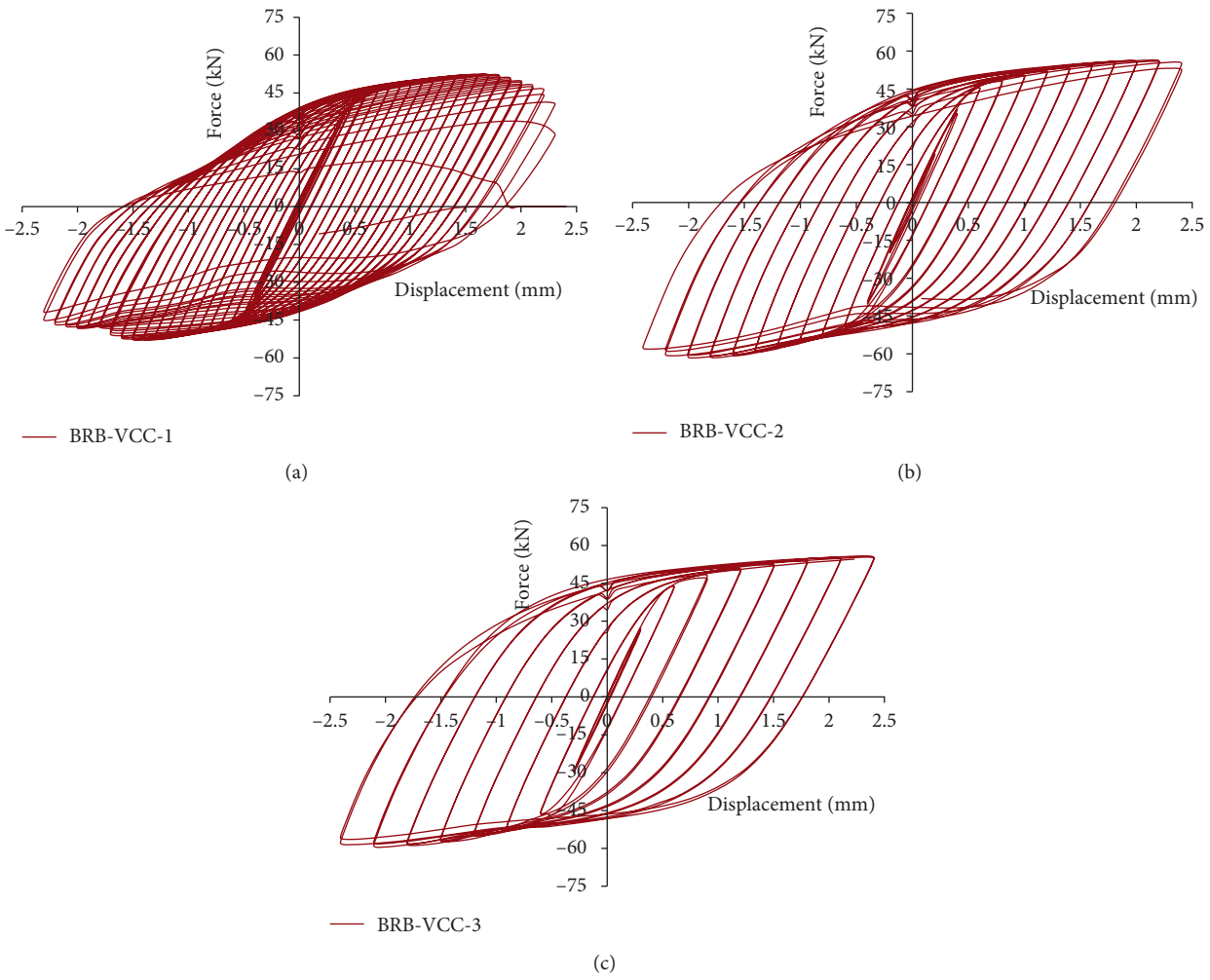

Figure 10: Hysteresis loops of S-I. (a) BRB-VCC-1. (b) BRB-VCC-2. (c) BRB-VCC-3.

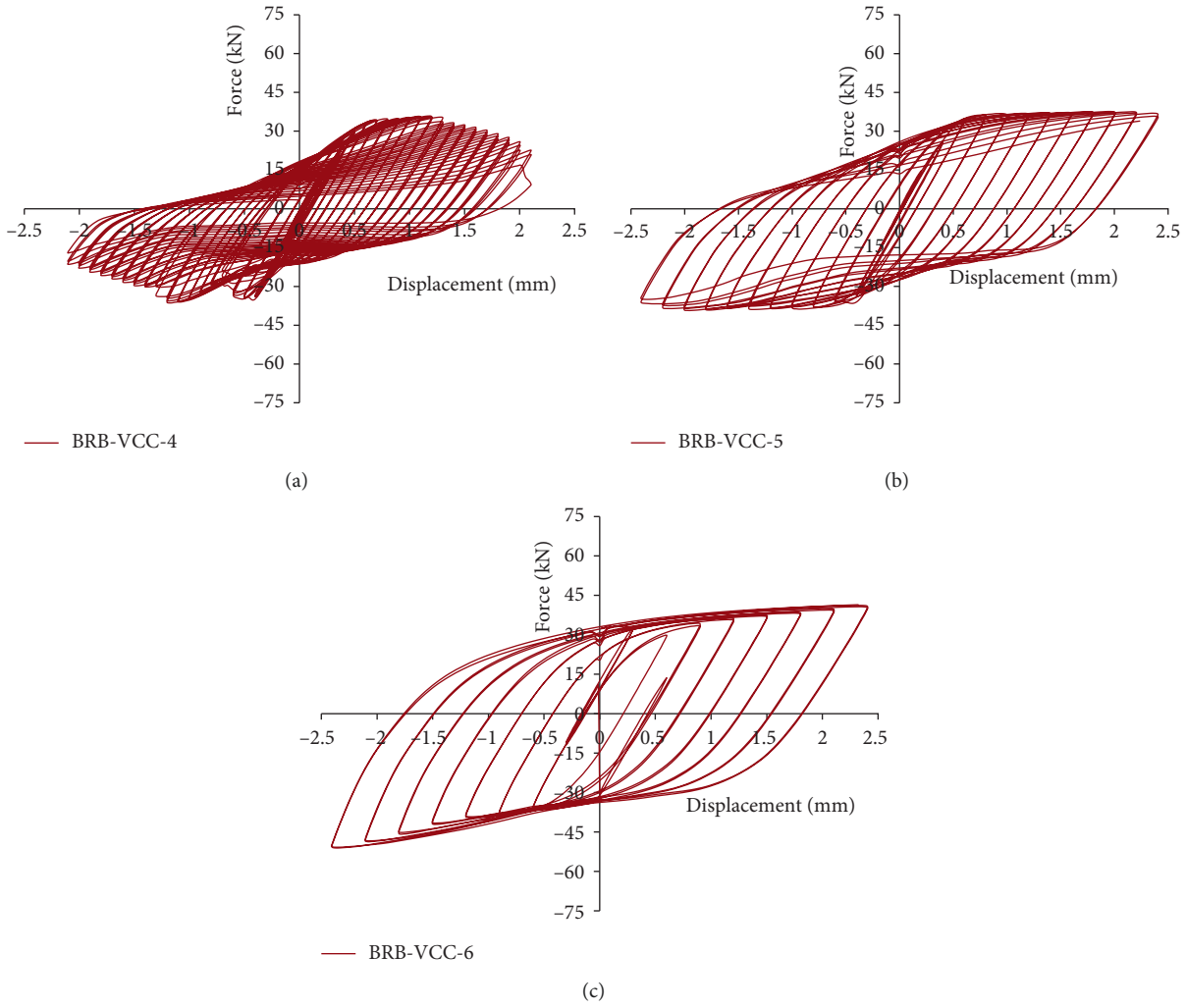

Figure 11: Hysteresis loops of S-II. (a) BRB-VCC-4. (b) BRB-VCC-5. (c) BRB-VCC-6.

dissipation capacities of the specimens are satisfactory. The hysteresis loop of BRB-VCC-1 is different from that of BRB-VCC-2 and BRB-VCC-3, and the hysteresis loop of BRB-VCC-4 is also different from that of BRB-VCC-5 and BRB-VCC-6. The primary reason is that BRB-VCC-1 and BRB-VCC-4 endured more loading circles, which led to more cumulative damage than other specimens in S-I and S-II, and the hysteresis loops of BRB-VCC-1 and BRB-VCC-4 pinch more severely.

5.3.3. Skeleton Curves. The skeleton curves of the six specimens are shown in Figure 12. It can be noted that the ductilities of the specimens are satisfactory. Table 3 lists the main mechanical parameters of the specimens. By comparing the specimens in two series, it is known that the axial capacity of BRB-VCC-1 is larger than that of BRB-VCC-4. It can be concluded that the capacity of entire BRB-VCC is bigger when the cross-sectional area of the flat-plate segment is bigger. The strength ratios $F_{c,u}/F_{t,u}$ of the specimens do not exceed 1.3, which satisfies the criteria for BRBs specified in section K3 of ANSI/AISC 341-10 [9].

6. Verification of Theory

Table 4 lists the main mechanical properties of the specimens, as obtained from the test and formulas. The experimental results agree well with the calculation results. Therefore, the suggested formulas can be considered reliable, and they can be used to predict the main mechanical parameters of BRB-VCCs in practical engineering.

7. Finite Element Analysis

7.1. Reliability of ABAQUS Analysis. Specimens are simulated using the ABAQUS software by employing the solid element C3D8R. The interaction between the core and the tube is simulated by defining the contact. The normal behavior of the contact is defined as "hard" contact, and the tangential behavior of the contact is smooth. The stress-strain relation of Q235B is bilinear in ABAQUS, and the material properties are listed in Table 2.

The hysteresis loops of BRB-VCC-3 by test and by ABAQUS are in good agreement, as shown in Figure 13,

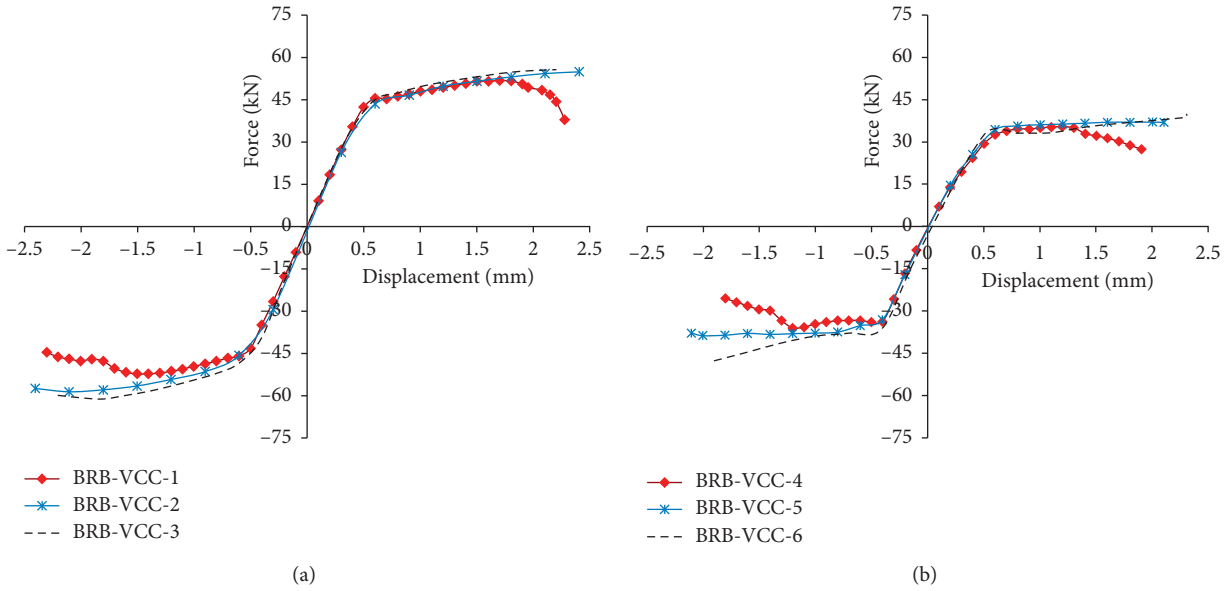

Figure 12: Skeleton curves of specimens. (a) S-I (b) S-II.

Table 3: Main experimental results of the specimens.

Series	Specimen	Tension			Compression			$F_{c,u}/F_{t,u}$
		$F_{t,u}$ (kN)	$\delta_{t,u}$ (mm)	Circles	$F_{c,u}$ (kN)	$\delta_{c,u}$ (mm)	Circles	
S-I	BRB-VCC-1	51.78	1.70	51	52.27	1.50	45	1.01
	BRB-VCC-2	55.65	2.21	33	61.19	1.80	27	1.10
	BRB-VCC-3	54.87	2.41	24	58.63	2.10	21	1.07
S-II	BRB-VCC-4	35.33	1.20	36	35.95	1.20	34	1.02
	BRB-VCC-5	37.02	2.00	30	38.75	2.01	29	1.05
	BRB-VCC-6	41.35	2.11	22	51.68	2.10	20	1.25

Table 4: Comparison of theoretical and test results.

Series	Specimen	k_e (kN/mm)			F_y (kN)			δ_y (mm)		
		Test	Formula	Error (%)	Test	Formula	Error (%)	Test	Formula	Error (%)
S-I	BRB-VCC-1	130.2	131.5	**0.10**	35.2	36.1	**2.74**	0.29	0.28	**1.82**
	BRB-VCC-2	133.5		**1.49**	36.0		**0.33**	0.30		**2.18**
	BRB-VCC-3	139.4		**5.63**	36.6		**1.33**	0.28		**4.36**
S-II	BRB-VCC-4	110.4	115.2	**4.19**	30.7	30.1	**1.83**	0.23	0.24	**4.16**
	BRB-VCC-5	115.6		**0.29**	31.5		**4.48**	0.24		**0**
	BRB-VCC-6	109.4		**5.02**	31.7		**5.02**	0.23		**4.16**

which proves that the FEM result is reliable. The Mises stress distribution of the restraining tube and core is shown in Figure 14, which demonstrates that the flat-plate segments indeed yield earlier than the rest of core.

7.2. Comparison with BRB-TJ-1

7.2.1. Design of Models. The BRB-VCCs are compared with a traditional TJ-I buckling-restrained brace (BRB-TJ-I) by FEM analysis. The BRB-TJ-I, invented by Professor G-Q Li at Tongji University, has been successfully applied in many important projects in China. The constitutions of BRB-TJ-I and BRB-VCCs are presented in Figure 15, and their geometric parameters are listed in Table 5. The steel used is Q235B, and the material properties are listed in Table 2.

The exact method for establishing the finite element model in this Section is the same as the method in Section 7.1. The whole model is shown in Figure 16.

7.2.2. Yield Regions in Models. The yield points of models can be identified by observing the dynamic images of parameter AC YIELD in software ABAQUS. For BRB-TJ-I, all regions of the core yield simultaneously when the axial force arrives at the yield capacity, as shown in Figure 17.

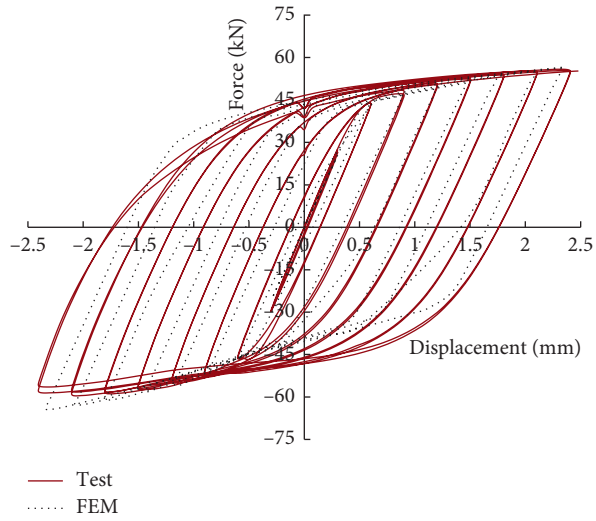

Figure 13: Comparison of hysteresis loops of BRB-VCC-3.

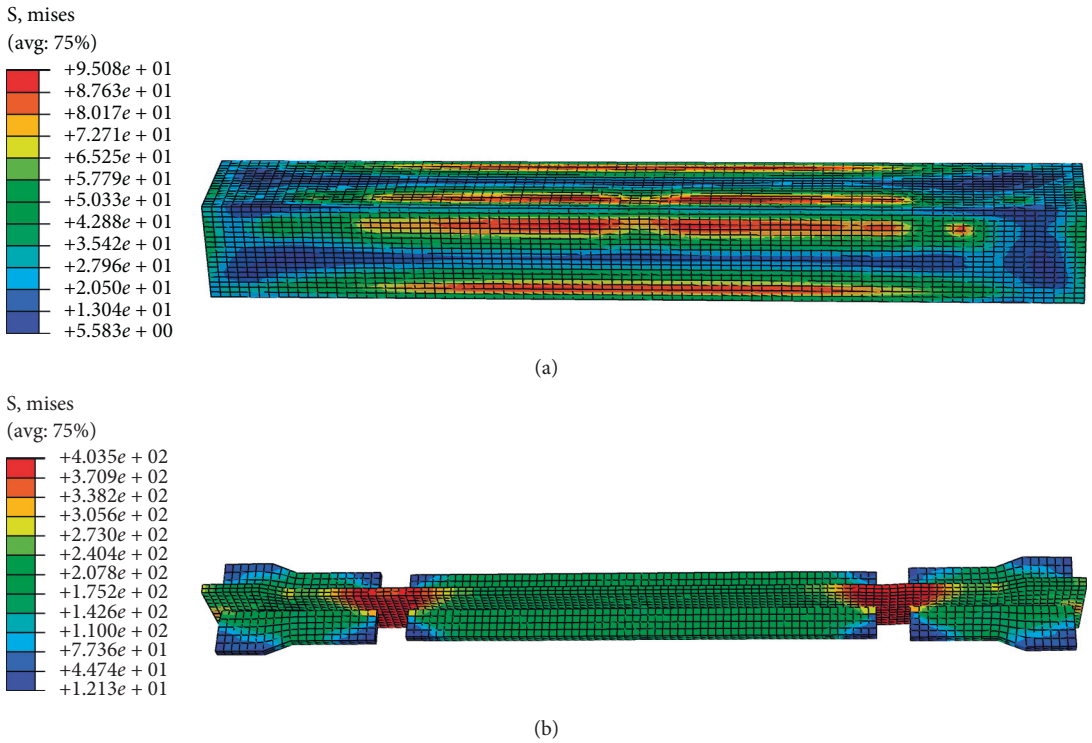

Figure 14: Mises stress contours of the specimen. (a) Restraining tube ($\sigma_{max} = 95.36\ N/mm^2 < f_y$). (b) Inner core ($\sigma_{max} = 403.5\ N/mm^2 > f_y$).

For BRB-VCCs, the flat-plate segment yields firstly while the rest of the segments of the core are still in elastic, as shown in Figures 18(a), 19(a), and 20(a). The stiffened-plate segments yield when the axial force arrived at its yield capacity, as shown in Figures 18(b), 19(b), and 20(b).

7.2.3. Comparing of Mechanical Performance. The hysteretic curves of models are shown in Figure 21. There is only one yield point in hysteretic curves of BRB-TJ-I, as marked clearly in Figure 21(a). Noticeably, there are two yield points in the curves of BRB-VCCs, and their exact positions have been marked in Figures 21(b)–21(d).

The main mechanical properties of the models are listed in Table 6. The following conclusions are found: (1) the yielding displacements of BRB-VCCs are approximately 73% compared to those of the BRB-TJ-I. (2) The interforces of BRB-VCCs increase faster than BRB-TJ-I after the yield of the flat-plate segment. (3) Different from the BRB-TJ-I, the hysteretic curves of BRB-VCCs show slight pinch after the second yield point, as shown in Figure 21.

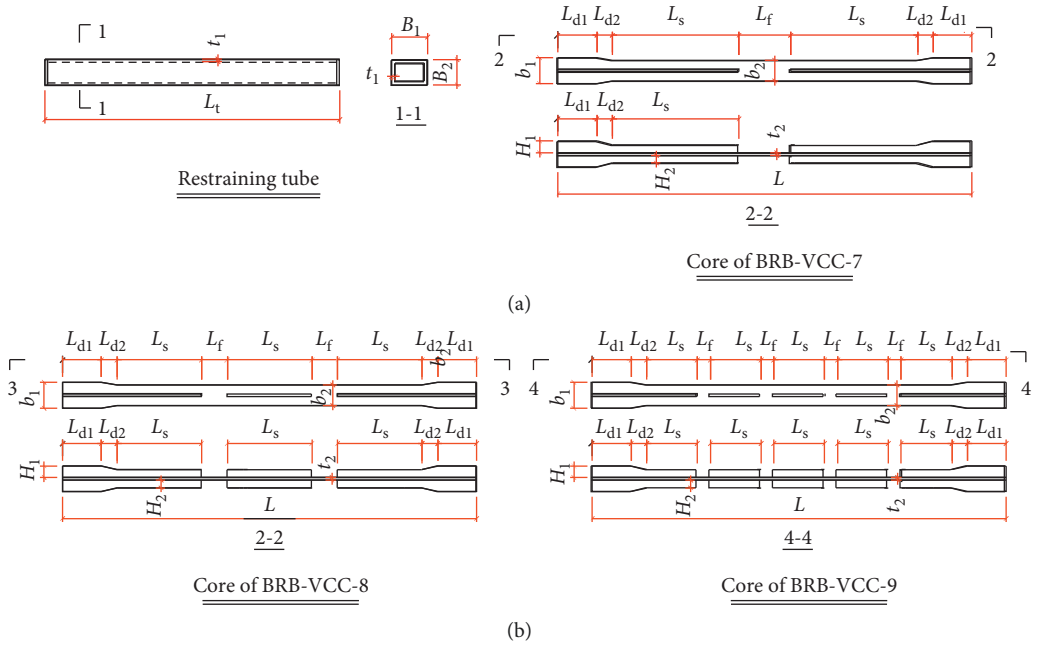

Figure 15: Model details. (a) BRB-TJ-I. (b) BRB-VCC.

Table 5: Design parameters of models (unit: mm).

Model	Restraining tube	Core	End rib	Middle rib	Flat-plate segment	
	$L_t \times B_1 \times B_2 \times t_1$	$L \times b_1 \times b_2 \times t_2$	$L_{d1} \times L_{d2} \times H_1 \times H_2 \times t_3$	$L_s \times H_2 \times t_3$	L_f	Number
BRB-TJ-I	$1080 \times 102 \times 94 \times 12$	$1600 \times 100 \times 80 \times 10$	$180 \times 60 \times 45 \times 30 \times 8$	—	—	—
BRB-VCC-7				$520 \times 30 \times 8$	80	1
BRB-VCC-8				$346 \times 30 \times 8$	40	2
BRB-VCC-9				$208 \times 30 \times 8$	20	4

Figure 16: Finite element model in software ABAQUS.

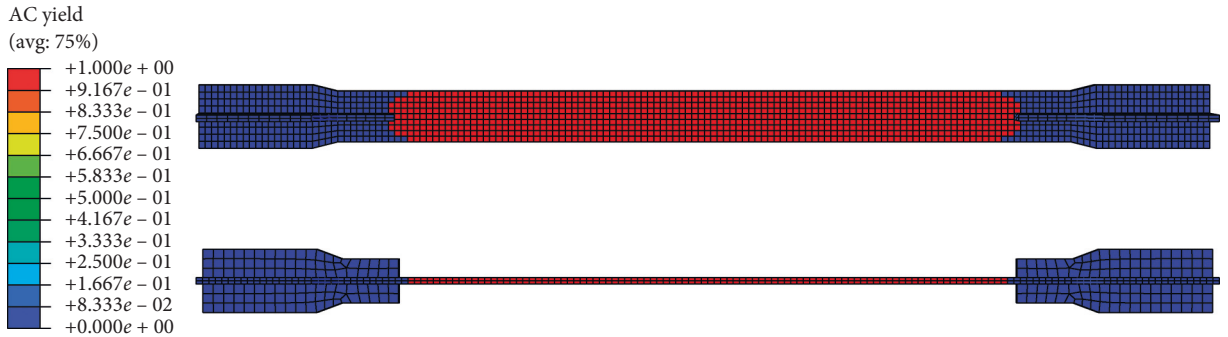

Figure 17: AC yield of the BRB-TJ-I core ($\delta_y = 1.86$ mm and $F_y = 195.6$ kN). Note: AC YIELD is 1.0 in the plastic region and is 0 in the elastic region.

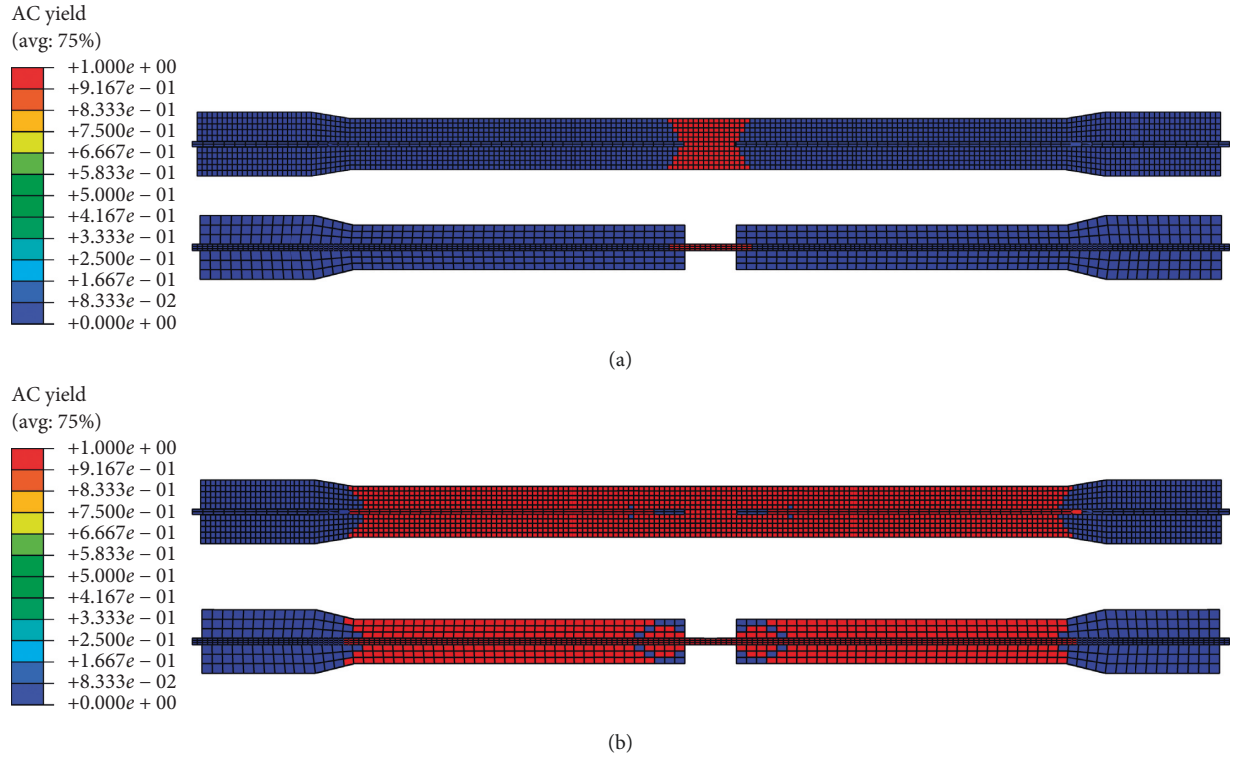

Figure 18: AC yield of the BRB-VCC-7 core. (a) Flat-plate segments yield firstly ($\delta_{y1} = 1.35$ mm and $F_{y1} = 201.6$ kN). (b) Stiffened-plate segments yield soon later ($\delta_{y2} = 1.52$ mm and $F_{y2} = 333.4$ kN). Note: AC YIELD is 1.0 in the plastic region and is 0 in the elastic region.

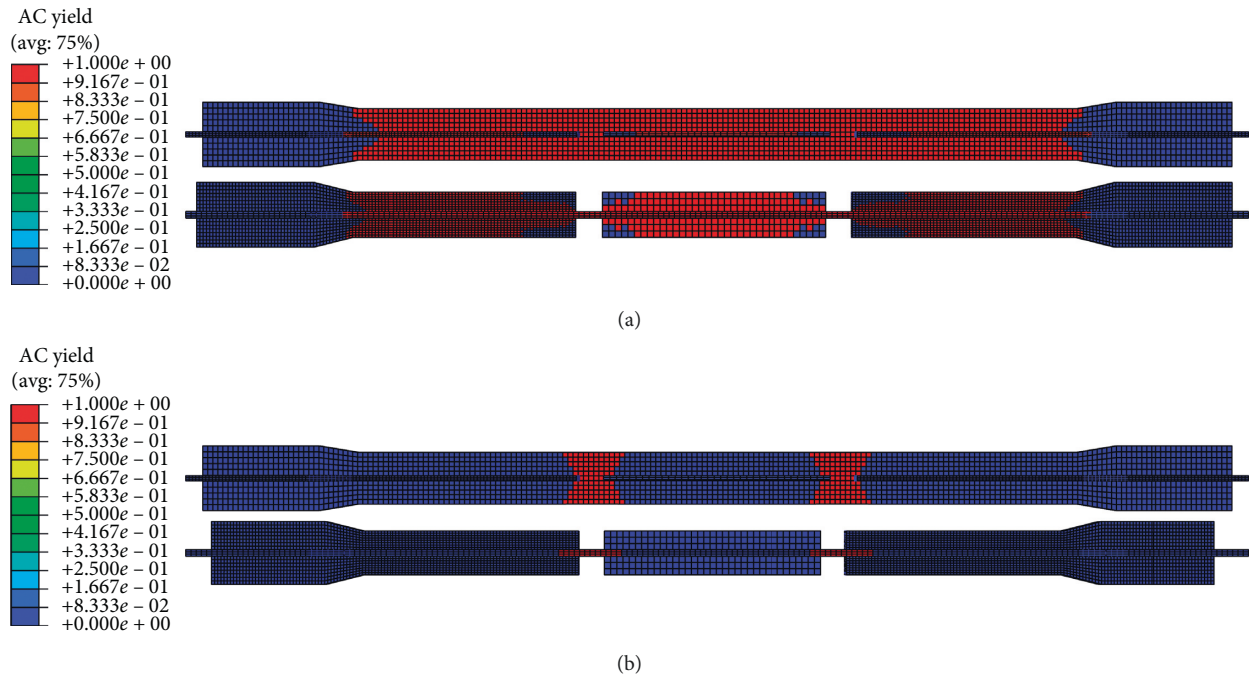

Figure 19: AC YIELD of the BRB-VCC-8 core. (a) Flat-plate segments yield firstly ($\delta_{y1} = 1.37$ and $F_{y1} = 198.4$ kN). (b) Stiffened-plate segments yield soon later ($\delta_{y2} = 1.81$and $F_{y2} = 325.9$ kN). Note: AC yield is 1.0 in the plastic region and is 0 in the elastic region.

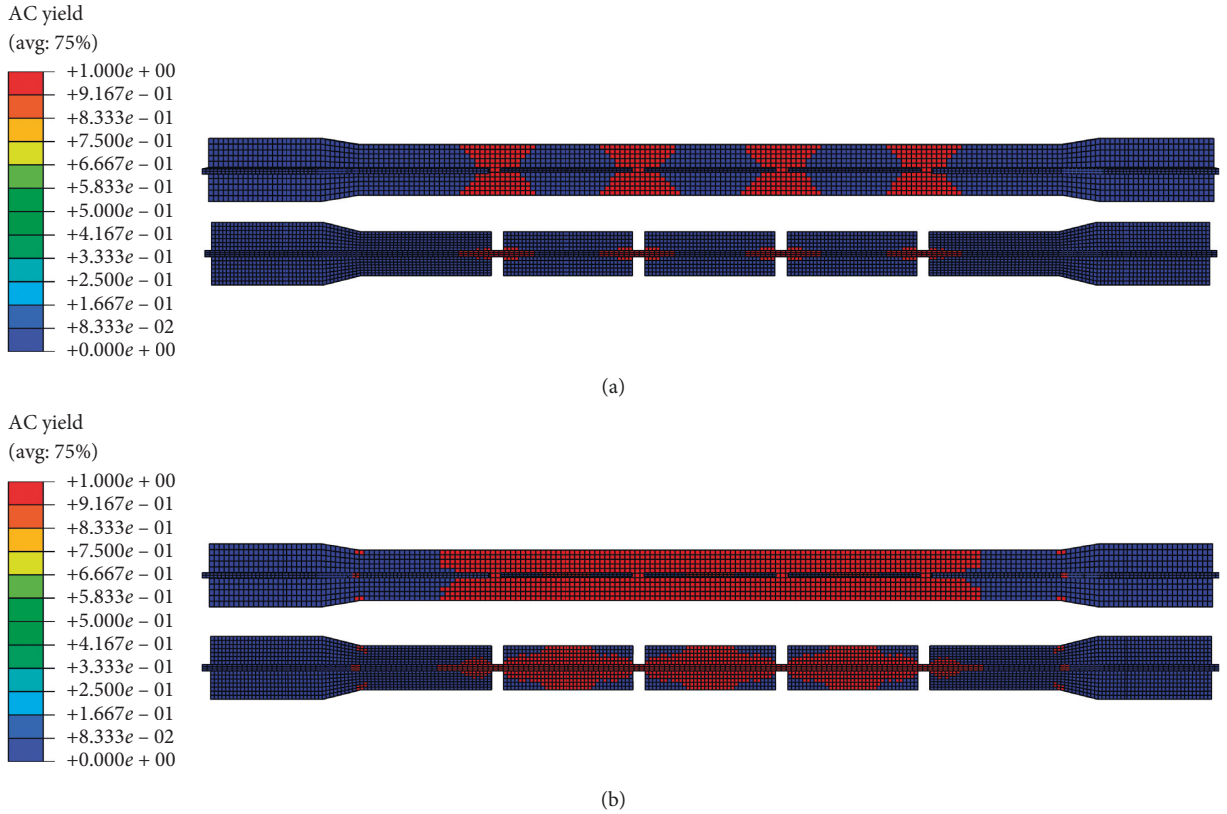

Figure 20: AC yield of the BRB-VCC-9 core. (a) Flat-plate segments yield firstly ($\delta_{y1} = 1.37$ mm and $F_{y1} = 224.2$ kN). (b) Stiffened-plate segments yield soon later ($\delta_{y2} = 1.92$ mm and $F_{y2} = 300.9$ kN). Note: AC YIELD is 1.0 in the plastic region and is 0 in the elastic region.

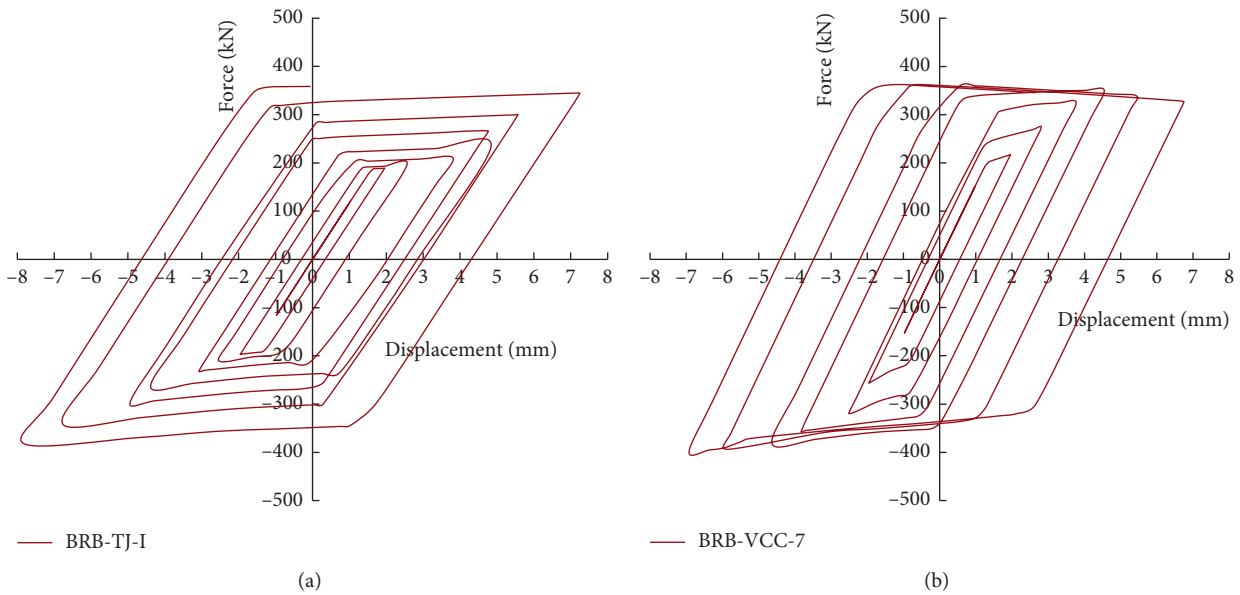

Figure 21: Continued.

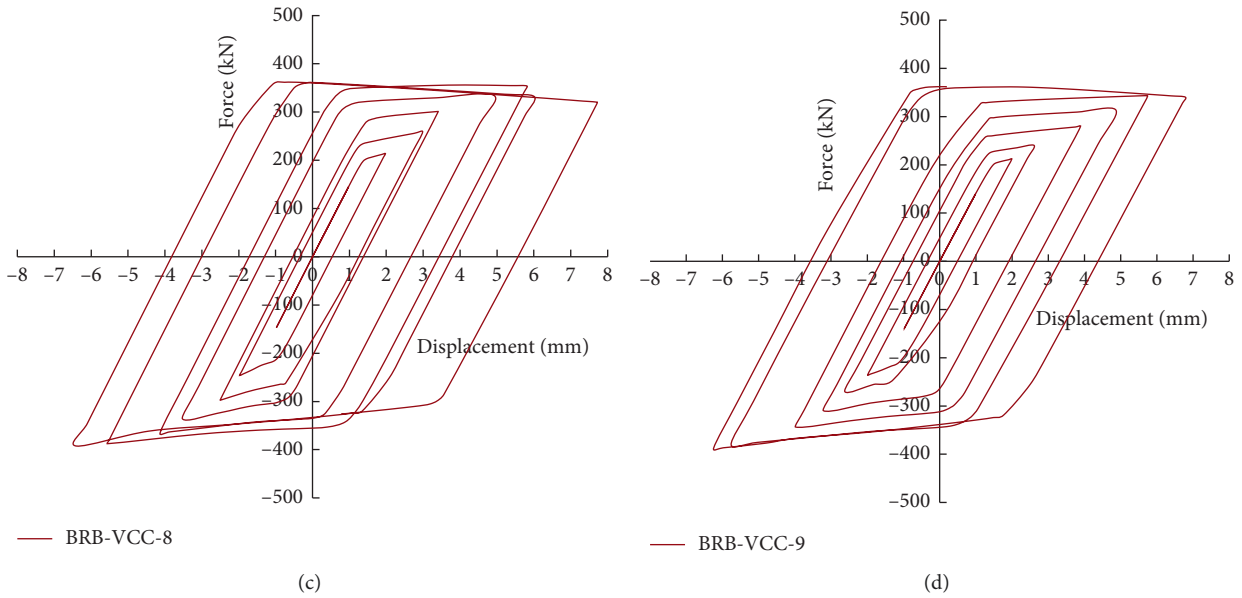

Figure 21: Hysteresis curves of models. (a) BRB-TJ-I. (b) BRB-VCC-7. (c) BRB-VCC-8. (d) BRB-VCC-9.

Table 6: Comparisons of FEM analysis results.

Model	k_e (kN/mm)	First yield point		Second yield point		Ratio of BRB-VCCs to BRB-TJ-I (%)		
		F_{y1}	δ_{y1}	F_{y2}	δ_{y2}	k_e	F_{y1}	δ_{y1}
BRB-TJ-I	117.8	195.6	**1.86**	—	—	—	—	—
BRB-VCC-7	154.9	201.6	**1.35**	333.4	1.52	1.31	1.03	**72.5**
BRB-VCC-8	148.5	198.4	**1.37**	325.9	1.81	1.26	1.01	**73.6**
BRB-VCC-9	141.2	200.2	**1.37**	300.9	1.92	1.20	1.02	**73.6**

8. Conclusions

According to the theoretical, experimental, and FEM study results obtained in this paper, the following conclusions can be drawn:

(1) The proposed design equations are reliable and can be used conveniently in practical engineering

(2) The hysteretic behaviours and ductilities of the BRB-VCC specimens are satisfactory, and the strength ratios $F_{c,u}/F_{t,u}$ of the specimens do not exceed 1.3, which satisfies the criteria for BRBs defined in section K3 of ANSI/AISC 341-10

(3) The yielding displacement of BRB-VCC is approximately 70% that of BRB-TJ-I, which may yield earlier than BRB-TJ-I in concrete structures under earthquake action

Data Availability

The data used to support the findings of this study are available from the corresponding author upon request by email: bright_li@chd.edu.cn.

Additional Points

(i) A new type of buckling-restrained brace with a variable cross-section core is presented. (ii) The theoretical formulas to predict the design parameters of the brace are derived; (iii) Tests are conducted to clarify the behaviour of the brace and prove the reliability of the equations; (iv) The behaviour of the proposed BRB is compared to that of a traditional BRB.

Conflicts of Interest

The authors declare that they have no conflicts of interest.

Acknowledgments

Binbin Li, who has provided valuable suggestion for specimen design, is gratefully acknowledged. The work reported hereinabove was financially supported by the National Science Foundation of China through project no. 51208057, the National Science Foundation of Shaanxi Province through project no. 2019JM-522, and the Basic Scientific and Research Foundation of Central Colleges through project no. 300102288104.

References

[1] H. M. Yazdi, M. Mosalman, and A. M. Soltani, "Seismic study of buckling restrained brace system without concrete infill," *International Journal of Steel Structures*, vol. 18, no. 1, pp. 153–162, 2018.

[2] S. P. Timoshenko, *Theory of Elastic Stability*, Science press, New York, NY, USA, 2nd edition, 1965.

[3] American Institute of Steel Construction (AISC), *Seismic Provisions for Structural Steel Buildings (ANSI/AISC 341-16)*, American Institute of Steel Construction, Chicago, IL, USA, 2016.

[4] M. Bosco, E. M. Marino, and P. P. Rossi, "Design of steel frames equipped with BRBs in the framework of Eurocode 8,"

Journal of Constructional Steel Research, vol. 113, pp. 43–57, 2015.

[5] G. Q Li, H. J. Jin, M. D. Pang, Y. W. Li, Y. Z. Sun, and F. F. Sun, Development of structural metal energy-dissipation techniques for seismic disaster mitigation of buildings," in *Proceedings of the 9th International Conference on Behavior Of Steel Structures in Seismic Areas (STESSA 2018)*, Christchurch, New Zealand, February 2018.

[6] A. Maurya, M. R. Eatherton, R. Matsui, and S. H. Florig, "Experimental investigation of miniature buckling restrained braces for use as structural fuses," *Journal of Constructional Steel Research*, vol. 127, pp. 54–65, 2016.

[7] M. Dehghani and R. Tremblay, "An analytical model for estimating restrainer design forces in bolted buckling-restrained braces," *Journal of Constructional Steel Research*, vol. 138, pp. 608–620, 2017.

[8] H. Eletrabi and J. D. Marshall, "Catenary action in steel framed buildings with buckling restrained braces," *Journal of Constructional Steel Research*, vol. 113, pp. 221–233, 2015.

[9] ANSI/AISC 341-10, *Seismic Provisions for Structural Steel Buildings*, American Institute of Steel Construction, Chicago, IL, USA, 2010.

[10] R. Tremblay, M. Dehghani, L. Fahnestock et al., "Comparison of seismic design provisions for buckling restrained braced frames in Canada, United States, Chile, and New Zealand," *Structures*, vol. 8, pp. 183–196, 2016.

[11] H. Wu, G. Zhou, and J. Zhao, "Seismic performance of existing RC frame structures reinforced with buckling-restrained braces," *China Civil Engineering Journal*, vol. 46, pp. 37–46, 2013.

[12] R. Bazaez and P. Dusicka, "Cyclic behavior of reinforced concrete bridge bent retrofitted with buckling restrained braces," *Engineering Structures*, vol. 119, pp. 34–48, 2016.

[13] L. Liang and G. Q. Li, "Simplified algorithm of buckling critical load for shear-bending cantilever rod under axially uniformly distributed load, xi'an univerxity of architecture and technology," *Nature Science*, vol. 45, no. 6, pp. 609–6141, 2013.

[14] Li Liang, *Design approach and seismic behavior study on novel multi-lateral resistant steel-concrete mixed structure*, Department of Civil Engineering, Tongji University, Shanghai, China, Dissertation of PhD, 2012.

[15] GB50017-2017, *Standard for Design of Steel Structures*, China Architecture & Building Press, Beijing, China, 2018.

[16] D. Hu, Li Guoqiang, and F. Sun, "Full-scale shaking table tests on a hinge-connected steel frame with buckling-restrained braces," *China Civil Engineering Journal*, vol. 43, pp. 37–46, 2010.

[17] M. Mirtaheri, A. Gheidi, A. P. Zandi, P. Alanjari, and H. R. Samani, "Experimental optimization studies on steel core lengths in buckling restrained braces," *Journal of Constructional Steel Research*, vol. 67, no. 8, pp. 1244–1253, 2011.

[18] S. A. R. Tabatabaei, S. R. Mirgghaderi, and A. Hosseini, "Experimental and numerical developing of reduced length buckling-restrained braces," *Engineering Structures*, vol. 77, pp. 143–160, 2014.

[19] M. Bruneau, S. El-Bahey, S. Fujikura, and D. Keller, "Structural fuses and concrete-filled steel shapes for seismic- and multi-hazard resistant design," *Bulletin of the New Zealand Society for Earthquake Engineering*, vol. 44, no. 1, pp. 44–52, 2011.

[20] H. Guerrero, T. Ji, A. Teran-Gilmore, and J. A. Escobar, "A method for preliminary seismic design and assessment of low-rise structures protected with buckling-restrained braces," *Engineering Structures*, vol. 123, pp. 141–154, 2016.

[21] F. Barbagallo, M. Bosco, E. M. Marino, P. P. Rossi, and P. R. Stramondo, "A multi-performance design method for seismic upgrading of existing RC frames by BRBs," *Earthquake Engineering & Structural Dynamics*, vol. 46, no. 7, pp. 1099–1119, 2017.

[22] A. Tena-Colunga and H. J. Nangullasmú-Hernández, "Assessment of seismic design parameters of moment resisting RC braced frames with metallic fuses," *Engineering Structures*, vol. 95, pp. 138–153, 2015.

[23] M. Bosco and E. M. Marino, "Design method and behavior factor for steel frames with buckling restrained braces," *Earthquake Engineering & Structural Dynamics*, vol. 42, no. 8, pp. 1243–1263, 2013.

[24] J.-S. Lei and L.-Y. Li, "Combined web distortional and lateral-torsional buckling of partially restrained I-section beams," *International Journal of Mechanical Sciences*, vol. 131-132, pp. 107–112, 2017.

[25] Z. Qu, J. Xie, T. Wang, and S. Kishiki, "Cyclic loading test of double K-braced reinforced concrete frame subassemblies with buckling restrained braces," *Engineering Structures*, vol. 139, pp. 1–14, 2017.

[26] M. Iwata, M. Midorikawa, and K. Koyano, "Buckling-restrained brace with high structural performance," *Steel Construction*, vol. 11, no. 1, pp. 3–10, 2018.

[27] L. Liang, L. Guoqiang, and L. Yu-Shu, "Simplified algorithm of the novel steel-concrete mixed structure under lateral load," *International Journal of High-Rise Buildings*, vol. 1, no. 4, pp. 247–254, 2012.